The Diameters of Frozen-hydrated Chromatin Fibers Increase with DNA Linker Length: Evidence in Support of Variable Diameter Models for Chromatin

Brian D. Athey, Michael F. Smith, Debby A. Rankert, Shawn P. Williams, and John P. Langmore

Biophysics Research Division and Department of Biological Sciences, The University of Michigan, Ann Arbor, Michigan 48109-2099

Abstract. The diameters of chromatin fibers from *Thyone briareus* (sea cucumber) sperm (DNA linker length, n = 87 bp) and *Necturus maculosus* (mudpuppy) erythrocytes (n = 48 bp) were investigated. Soluble fibers were frozen into vitrified aqueous solutions of physiological ionic strength (124 mM), imaged by cryo-EM, and measured interactively using quantitative computer image-processing techniques. Frozen-hydrated *Thyone* and *Necturus* fibers had significantly different mean diameters of 43.5 nm (SD = 4.2 nm; SEM = 0.61 nm) and 32.0 nm (SD = 3.0 nm; SEM = 0.36 nm), respectively. Evaluation of previously published EM data shows that the diameters of chromatin from a large number of sources are proportional to linker length. In addition, the inherent variability in fiber diameter suggests a relationship between fiber structure and the heterogeneity of linker length. The cryo-EM data were in quantitative agreement with space-filling double-helical crossed-linker models of *Thyone* and *Necturus* chromatin. The data, however, do not support solenoid or twisted-ribbon models for chromatin that specify a constant 30 nm diameter. To reconcile the concept of solenoidal packing with the data, we propose a variable-diameter solid-solenoid model with a fiber diameter that increases with linker length. In principle, each of the variable diameter models for chromatin can be reconciled with local variations in linker length.

Most of the DNA within the nucleus of eukaryotic cells is packaged into "30-nm" chromatin fibers (reviewed by Crane-Robinson et al., 1984; Felsenfeld and McGhee, 1986; Pederson et al., 1986; Koch, 1989; Widom, 1989; van Holde, 1989). Low-angle x-ray diffraction studies of living cells, intact nuclei, and isolated chromosomes have shown that these "thick fibers" exist in vivo, where they are packed together in a side-by-side manner (Langmore and Shutt, 1980; Langmore and Paulson, 1983; Paulson and Langmore, 1983). X-ray studies of chromatin gels and of soluble fibers have also demonstrated that thick fiber structure can be preserved in vitro (Sperling and Klug, 1977; Widom and Klug, 1985; Williams et al., 1986).

The fundamental repeating subunit of chromatin is the nucleosome. This repeat was first visualized at low ionic strength by EM of unraveled chromatin fibers, which resembled "beads-on-a-string" (Olins and Olins, 1974; Woodcock et al., 1976). The "bead" is the nucleosome core particle, composed of a conserved amount (146 bp) of B-form DNA wrapped into 1.75 turns of a left-handed superhelix at a radius of 4.3 nm around a highly conserved histone protein octamer (Richmond et al., 1984). Core particles are connected to one another by linker DNA (the "string"), which varies in "linker length" from 20–95 bp (7–32 nm) depending on species and tissue (Kornberg, 1977). If the very lysine-rich histone, H1, is bound to the beads-on-a-string structure at low ionic strength, the linker DNA becomes straight, and chromatin appears as a characteristic "zig-zag" ribbon structure, as visualized by EM (Thoma and Koller, 1977).

Although the structure of the nucleosome core particle is known to 0.7 nm resolution (Richmond et al., 1984), it is not yet understood how the zig-zag ribbon is folded to form the chromatin thick fiber. Many x-ray studies have suggested that the nucleosomal interactions within the folded fiber are conserved, independent of linker length (Langmore and Paulson, 1983; Widom et al., 1985; Williams et al., 1986; Koch et al., 1987, 1988). It is not known, however, whether the diameter of the thick fiber is also conserved. Although some hydrodynamic studies have concluded that the diameter of the chromatin fiber is constant (McGhee et al., 1983; Butler, 1984), x-ray studies have concluded that fiber diameter increases with linker length (Williams et al., 1986; Koch et al., 1988). Although solution studies are able to measure the average behavior of bulk chromatin in a native environment, they are subject to potential artifacts of interpretation due to uncertainties in molecular hydration, flexibility, shape, intramolecular aggregation, and heterogeneity of structure. Some EM studies report a constant ~30 nm diameter, (Widom et al., 1985; Lowary and Widom, 1989), whereas others report an increase in fiber diameter with linker length (Williams et al., 1986; Alegre and Subirana, 1989; Smith et al., 1990). Although conventional microscopy is able to

make accurate measurements of the diameters of a few images of individual fibers, they are subject to potential artifacts of dehydration and staining (e.g., Anderson, 1951; Nermut, 1972).

The examination of unstained, frozen-hydrated chromatin fibers using cryo-EM combines the virtues of conventional EM and solution studies, by studying individual molecules in their native, aqueous environment. Assumptions need not be made about hydration, flexibility, shape, aggregation, or homogeneity of structure. Frozen-hydrated molecules are known to retain their native conformation to high resolution (reviewed by Dubochet et al., 1988; Lepault, 1985). With specific reference to the preservation of diameter in the frozen-hydrated state, Olson and Baker (1989) demonstrated that diameters of cryopreserved virus particles were within 3% of those obtained from x-ray scattering. In contrast, diameter measurements of conventionally prepared virus particles were up to 31% smaller than x-ray measurements (Earnshaw et al., 1978).

An unambiguous answer to the "fiber diameter question" will affect the direction of future structural experiments and chromatin model-building studies. Therefore, the diameters of *Thyone* sperm chromatin (linker length, $n = 87$ bp) and of *Necturus* erythrocyte chromatin ($n = 48$ bp) were investigated by cryo-EM. Soluble fibers were frozen as vitrified aqueous solutions of physiological ionic strength (124 mM), imaged using cryo-EM, and measured using quantitative computer image processing. The results indicated a diameter difference of ~12 nm, suggesting a direct relationship between fiber diameter and DNA linker length. Analysis of previously published EM data regarding chromatin fiber diameter agrees with this hypothesis. Only chromatin fiber models specifying a diameter that increases with linker length are supported by these findings.

Materials and Methods

Buffers

Wash buffer (WB) consisted of 130 mM NaCl, 5.0 mM KCl, 2.0 mM $MgCl_2$, 10 mM HEPES (pH 7.0), and 0.1 M sucrose. Synthetic Sea Water (SSW) was prepared from a powder obtained from Instant Ocean (East Lake, OH). Buffer A contained 60 mM KCl, 15 mM NaCl, 15 mM PIPES (pH 7.0), 0.5 mM spermine, 0.5 mM spermidine, 2.0 mM EDTA, and 0.02% NaN_3. Buffer EB contained 60 mM KCl, 15 mM NaCl, 15 mM PIPES (pH 7.0), 3.0 mM EDTA, 0.1 mM PMSF, and 0.02% NaN_3. Micrococcal nuclease digestion buffer (MNase DB) was the same as EB, except EDTA was replaced by 0.5 mM $CaCl_2$ and 0.25 mM $MgCl_2$. Buffer MB was also the same as EB, except EDTA was replaced by 3 mM $MgCl_2$.

Isolation of Nuclei

Erythrocytes from *Necturus maculosus* (Charles Sullivan Inc., Nashville, TN) were obtained by heart puncture. Sperm from *Thyone briareus* (Woods Hole Marine Biological, Woods Hole, MA) were obtained in sea water from minced gonads. All subsequent steps were performed at 4°C, and all washes were to volumes at least 10 times that of the pellet. Except where noted, *Necturus* erythrocytes and nuclei were centrifuged for 6 min at 50 *g* during the washing steps. Erythrocytes were washed two times in WB, with the buffy coat removed to eliminate lymphocytes. The erythrocytes were then incubated for 1 h on ice in WB with 3 mM iodoacetate, and 0.2 mM PMSF to inhibit proteases. Living sperm were washed two times in SSW (20 min at 800 *g*) and were incubated for 1 h on ice in buffer A with 1 M sucrose, 3 mM iodoacetate, and 0.2 mM PMSF. *Thyone* sperm were then pelleted for 10 min at 200 *g*. Subsequent steps were very similar for both tissues. Cells were washed three times in buffer A with 0.1% digitonin, 1 mM iodoacetate, and 0.1 mM PMSF, and three times buffer A with 0.1% NP-40, 1 mM iodoacetate, and 0.1 mM PMSF. Nuclei were resuspended to 1 mg/ml in buffer A with 50% glycerol and quickly frozen by placing 1-ml aliquots within Eppendorf centrifuge tubes into a solution of methanol/dry ice. Nuclei were stored at −70°C.

Isolation of Chromatin

All steps were carried out in 1-ml vol. *Thyone* were always centrifuged for 10 min at 180 *g*; *Necturus* for 6 min at 50 *g*. 1-mg aliquots of nuclei were pelleted at 4°C, resuspended in MB, and then washed with MNase DB. Nuclei were then resuspended in MNase DB and incubated at 22°C for 5 min. Nuclei were digested with 20 U micrococcal nuclease (Worthington Biochemical Corp., Freehold, NJ) for 3 (*Thyone*) or 5 (*Necturus*) min, in order to solubilize chromatin of comparable molecular weights. Digestion was stopped by addition of EGTA to 5.0 mM and $MgCl_2$ to 1.0 mM. Nuclei were then pelleted and resuspended in 5.0 mM EDTA, pH 7.0, 0.1 mM PMSF in order to solubilize chromatin. Nuclei were allowed to lyse at 4°C for 30 min to 1 h, and then spun for 10 min in an Eppendorf centrifuge to pellet debris. Yields were 10–15% for *Thyone*, and 15–20% for *Necturus*. Chromatin was brought to physiological ionic strength by adding 1/10 vol 10 × EB. Final sample concentrations were typically 100–200 μg/ml. The use of EB allows for direct comparison with our other studies of chromatin fiber diameter (Williams et al., 1986; Smith et al., 1990; Williams, S. P., and J. P. Langmore, manuscript submitted for publication). Gel electrophoresis was performed to determine that typical *Thyone* and *Necturus* soluble fiber specimens had mass averages of 134 and 196 nucleosomes, respectively (data not shown). The average linker lengths of soluble chromatin from *Thyone* and *Necturus* (87 and 48 bp, data not shown) were identical to those found previously for nuclei (Williams et al., 1986). The fibers were fixed in EB at 4°C with 1% glutaraldehyde for ~24 h. It was observed previously (Dubochet et al., 1988), and verified during the course of this study, that unfixed chromatin fibers are sensitive to denaturation at the air-buffer interface, and are thus difficult to visualize in the frozen-hydrated state.

Cryo-EM

Specimens were prepared and transferred using standard techniques (Dubochet et al., 1988) as follows: holey plastic films (Fukami and Kôichi, 1965) were placed onto 400 mesh grids, carbon was vacuum evaporated onto both sides, and the grids were glow discharged. A 5-μl aliquot of undiluted chromatin in EB was applied to the grids, quickly blotted, and plunged into liquid ethane using a guillotine device. Frozen-hydrated tobacco mosaic virus (TMV)[1] specimens were prepared using a 1 mg/ml solution in water. All freezing was done in a cold room; grids were stored in liquid nitrogen before use.

Bright-field images were recorded at 33,000 times magnification at 80 KeV using a 100 μm objective aperture. Kodak SO-163 was developed in full-strength D-19 for 12 min. The cold stage was maintained at ~115° K during examination. Drift rates were usually 0.2–0.4 nm/s, caused by fluctuations in the ambient temperature. Most of the inelastically scattered electrons were filtered from the images by a spectrometer slit that had an effective width of 20 eV, thus increasing image contrast about threefold. Specimen areas with vitreous ice were located at 3,000 times magnification. The microscope was focused at 85,000 times magnification on an area ~13 μm from the area of interest. Modifications to the microdose focusing system allowed for the preirradiation of the imaged area to be $<3 \times 10^{-4}$ electrons/nm^2. Two low-dose images were made of the specimen area, each recorded for 3 s with an incident intensity of 200–300 electrons/nm^2/s. The first image was recorded as close to focus as possible, and was used for the diameter measurements. The second image was intentionally underfocused by a specific amount, usually 2,880 nm. The positions of the zeros in the phase contrast transfer function (CTF) of the second image were obtained by optical diffraction. These values were used to determine defocus of the second image and to calculate the defocus of the first image. The defocus for the *Thyone*, *Necturus*, and TMV data sets were 230–2,000 nm (mean = 1,280 nm), 320–1,900 nm (mean = 1,220 nm), and 0–1,000 nm (mean = ~500 nm), respectively. In addition, seven frozen-hydrated TMV fibers that were included with the *Necturus* specimen were measured. These images were defocused by 960–1,500 nm (mean = 1,370 nm). Ice thicknesses were calculated assuming an H_2O density of 0.92 g/cm^2 and mean free

1. *Abbreviations used in this paper*: CTF, phase contrast transfer function; FWHM, full width at half maximum; STEM, scanning transmission EM; TMV, tobacco mosaic virus.

paths of 280 nm for elastically scattered electrons and 207 nm for inelastically scattered electrons.

Magnification Determination

A 21,600 lines/cm square grating was the external standard used for all experiments (Ted Pella Co., Tustin, CA); calibrations were done at 115° K. The grating was measured in orthogonal directions to verify an isotropic specimen magnification. TMV fibers were used as an internal standard in a subset of the samples, and the 2.3-nm repeat was measured by computed Fourier transformation.

Image Processing

Image densities were recorded as 1024 × 1024 pixel areas using a Bioimage Visage-2000 image processing system (Bioimage Corp., Ann Arbor, MI). This array was subsequently compressed to 512 × 512 pixels, with the final pixel size being 1.0 nm on the specimen. Magnification calibration was ensured by recording an image of a 0.1-mm reticule in the micrograph plane. Subsequent interactive image-processing steps were performed on a Silicon Graphics IRIS 2500T workstation (Silicon Graphics, Mountain View, CA) using the EMPRO program package (Smith et al., 1990).

Chromatin fibers were chosen for measurement after visual examination of the digitized infocus and defocused micrographs. Only straight regions of fiber that exhibited a uniform diameter were analyzed. Slightly curved fibers of uniform diameter were straightened using a spline-fitting algorithm before analysis (12% of the frozen-hydrated fibers analyzed). Frozen-hydrated chromatin fiber segments were at least 21 nm in length, with a mean length of 49 nm. No region closer than 10 nm to the fiber ends was analyzed. Approximately 10–20% of the chromatin fibers in any given field met these selection criteria.

Fiber-axis orientation was estimated interactively and then digitally refined based on the local twofold symmetry of the fiber segment. Projections were obtained by summation of the mass thickness along the refined axis. This calculation was made (independently) three times for each fiber segment. These three projections were averaged in order to minimize spurious peaks in background intensity near the fiber edge. These average projections were used in all subsequent diameter measurement steps.

Fiber diameters were calculated from projections using the FORTRAN program DIAMETER. First, visual examination of each projection was performed and those having an asymmetric background intensity were discarded (12% of the projections). The projections were then smoothed by three-point averaging and folded about their center of symmetry. Next, the average background intensity was calculated using an area directly adjacent to the fiber, typically ~40-nm-wide areas along both sides the fiber. This average background intensity value was then subtracted from the projection. Next, the width of each projection at 15% of maximum mass thickness was measured. This measurement was found to provide a reasonable estimate of the diameter of unstained freeze-dried TMV (Smith et al., 1990), and gave an accurate value for the diameter of frozen-hydrated TMV in this study. Greater than 98% of the fiber mass was included within the 15% point. The full width at half maximum (FWHM) mass thickness was also measured.

The final frozen-hydrated data set included measurements from 46 *Thyone* and 69 *Necturus* close-to-focus fiber segments, as well as from 42 TMV segments. This corresponded to 2,350, 3,250, and 3,810 nm of combined fiber length, respectively.

Statistical Analysis

Statistical analyses were performed using the StatView program package (BrainPower Inc., Calabasas, CA). The diameter distributions of *Thyone*, *Necturus*, and TMV were compared using the *t* test. A linear regression was performed to relate diameter measurements to microscope defocus, ice thickness, and linker length; r_c is defined as the linear correlation coefficient. Tables were used to find the probability, $P_c(r_c,n)$, of exceeding r_c in a random sample of n observations taken from an uncorrelated parent population (Bevington, 1969).

Chromatin Fiber Models

Nucleosome core particles were built on a Silicon Graphics IRIS 2500T. The coordinate set was produced using the published dimensions of the core particle (Richmond et al., 1984). Ribbons with a $\Delta L = -2$ per nucleosome linking number increment were modeled with linker lengths of 87 and 48 bp. The DNA diameter was assumed to be 2.5 nm. The variable pitch and twist models were produced according to the pattern described by Williams et al. (1986). Final graphic display utilized the MIDAS program package (Ferrin et al., 1988). Diameters (edge-to-edge) of cylindrically averaged projections of these computer-generated models were measured using the program DIAMETER as described above. The hollow-solenoid (McGhee et al., 1983) and twisted-ribbon (Woodcock et al., 1984) physical models were built to scale (Williams et al., 1986).

Computer Modeling of EM Defocus

To determine the effect of EM defocus upon the measurement of fiber diameter, projections were made of uniform cylinders of 45, 31, and 17 nm diameter. The equation used for the CTF (Erickson and Klug, 1971) was based upon the 7% amplitude contrast observed for frozen-hydrated specimens embedded in thin ice (Toyoshima and Unwin, 1988); the CTF resolution cutoff was set to 1.0 nm^{-1}. The model projections were Fourier transformed and each multiplied by a series of CTFs ranging from −1,000 (overfocus) to +5,000 nm (underfocus). Modified projections were then generated by inverse Fourier transformation and their estimated diameters were determined using the program DIAMETER. Similar defocus tests were also performed using projections of the *Thyone* and *Necturus* computer models.

Results

EM Underfocus Has a Negligible Effect upon the Diameter Measurement of Close-to-Focus Fibers

Fig. 1 shows representative images of frozen-hydrated chromatin and TMV, showing the morphology of the fibers and the effects of defocus. Diameter determinations by microscopy are subject to potential systematic error due to the Fresnel fringes in the images. To test the effects of defocus upon the measurements, projections of solid cylinders were computationally modified by different amounts of defocus and measured using the computer program. Fig. 2 shows the percentage error in diameter measurement as a function of defocus. Between 0–2,000 nm underfocus measurements of the defocus-modified 45- and 31-nm cylinders were within 4% of the actual model diameters. Therefore, only the chromatin images in this range of defocus were analyzed. Nearly identical results were obtained when projections of the *Thyone* and *Necturus* chromatin computer models were used (data not shown). Between 0–1,500 nm underfocus, the 17-nm diameter model cylinder diameter was underestimated by <5%. Therefore, only the TMV control specimen images in this range of underfocus were analyzed. The predicted dependence of estimated diameter upon defocus was in quantitative agreement with the observed differences between measurements of in-focus and intentionally defocused *Necturus* fibers (data not shown).

Frozen-Hydrated Thyone and Necturus Chromatin Fibers Have Significantly Different Diameters

Fig. 3 shows histograms of the diameter measurements. The estimated diameters of *Thyone*, *Necturus*, and TMV were 43.5 nm (SD = 4.2 nm; SEM = 0.61 nm), 32.0 nm (SD = 3.0 nm; SEM = 0.36 nm), and 18.1 nm (SD = 0.9 nm; SEM = 0.14 nm), respectively. FWHM diameters were 33.7 nm (SD = 4.2 nm; SEM = 0.62 nm), 25.6 nm (SD = 3.7 nm; SEM = 0.45 nm), and 15.2 nm (SD = 0.9 nm; SEM = 0.14 nm) for *Thyone*, *Necturus*, and TMV, respectively. Strong evidence that the chromatin diameter distributions were different was indicated by the *t* test ($p < 10^{-4}$).

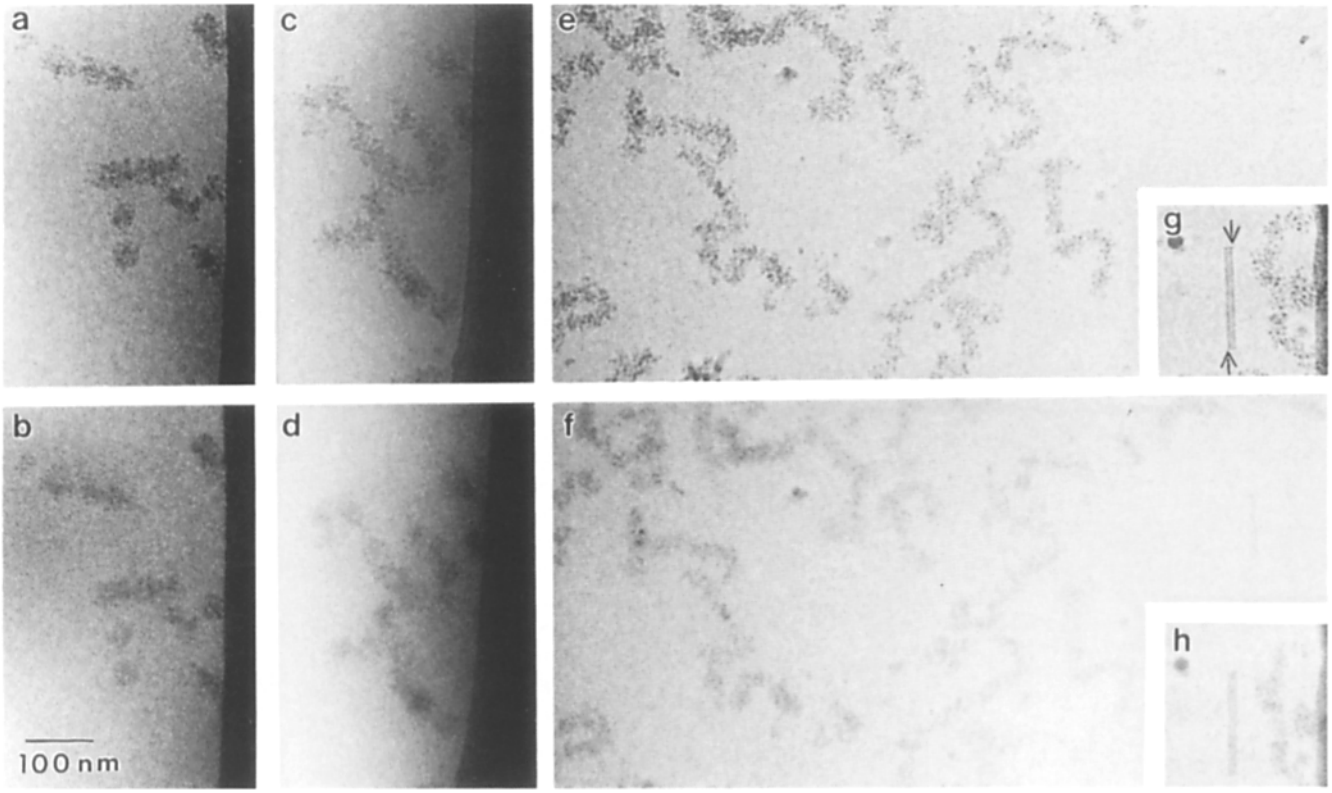

Figure 1. Electron images of frozen-hydrated chromatin and TMV fibers at two values of underfocus. (*a* and *b*) *Thyone* fibers (3,500 and 1,600 nm underfocus); (*c* and *d*) *Thyone* fibers (2,350 and 430 nm underfocus); (*e* and *f*) *Necturus* fibers (4,480 and 1,600 nm underfocus); the insets (*g* and *h*) show a TMV particle (with *Necturus* fibers) (5,300 and 1,500 nm underfocus). Fresnel fringes along the TMV are indicated by arrows. Bar, 100 nm.

Within the small range of defocus used for the diameter measurements, no correlation was found between estimated diameter and defocus (*Thyone* slope = 6.3×10^{-4} nm/nm, SE = 1.0×10^{-3} nm/nm, $r_c = 0.13$; *Necturus* slope = 2.5×10^{-4} nm/nm, SE = 8.6×10^{-4} nm/nm, $r_c = 0.04$). The range of ice thickness in the chromatin data set was 90–295 nm (*Thyone* mean = 181.7 nm, SD = 52.1 nm; *Necturus* mean = 129.0 nm, SD = 30.1 nm). No correlation between estimated diameter and ice thickness could be detected (*Thyone* slope = -4.4×10^{-3} nm/nm, SE = 1.2×10^{-2} nm/nm, $r_c = 0.06$; *Necturus* slope = 1.4×10^{-2} nm/nm, SE = 1.2×10^{-2} nm/nm, $r_c = 0.15$).

Discussion

The Observed Diameter Difference between Thyone and Necturus Chromatin Is Not Due to Artifacts of Cryo-EM or Image Processing

Cryo-EM is the most accurate method for determining macromolecular dimensions by EM (Olson and Baker, 1989). Nevertheless, systematic errors from fiber flattening, defocus, and image processing should be ruled out. Lepault (1985) and Kellenberger et al. (1986) failed to observe flattening of specimens preserved in the frozen-hydrated state, except in cases where the ice was thinner than the particles. In this present study, the ice thickness was always at least twice the diameter of the fibers. In addition, no statistical correlation was found between ice thickness and diameter. Artifacts of defocus were also insignificant, as seen by computer modeling and by statistical analysis of the data. Systematic errors in image processing were also insignificant. In principle, curved fibers or incorrect axes of projection could cause overestimation of the diameter. However, there was good correspondence between the estimated diameter of frozen-hydrated TMV (18.1 nm) and the value of 18.0 nm from x-ray scattering (Stubbs et al., 1977). Any such systematic overestimation of diameters would have affected the *Necturus* data more than the *Thyone* data, because the *Necturus* fibers had less contrast and were more curved.

Previous X-ray and EM Studies Indicate That Chromatin Diameter Increases with Linker Length

X-ray Studies. X-ray and neutron scattering are usually considered to be the most reliable methods for studying biologi-

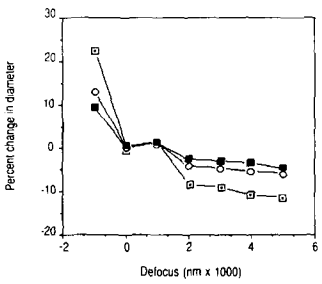

Figure 2. Variation in the estimated diameter of model cylinders as a function of focus. (*a*) 45.0-nm model (■); (*b*) 31.0-nm model (○); and (*c*) 17.0-nm model (⊡). Positive values along the abscissa correspond to underfocus.

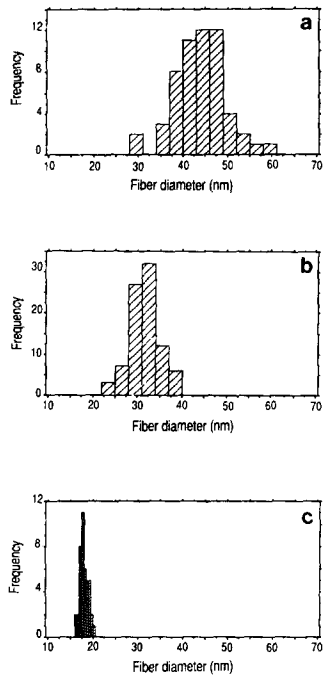

Figure 3. Histograms of estimated diameter measurements of close-to-focus frozen-hydrated fiber images. (*a*) *Thyone* (mean = 43.5 nm; SD = 4.2 nm; SEM = 0.61 nm); (*b*) *Necturus* (mean = 32.0 nm; SD = 3.0 nm; SEM = 0.36 nm); and (*c*) TMV (mean = 18.1 nm; SD = 0.9 nm; SEM = 0.14 nm).

cal molecules in solution. Guinier analysis of very low-angle scattering is a model-independent method to determine fiber diameter. However, it is subject to potential errors of interpretation due to undetected heterogeneity of structure, intramolecular aggregation, and failure of the assumption that the fibers are solid cylinders. Analysis of the higher-angle scattering gives information about the internal structure of the fibers, and in certain cases, information about the diameter.

Guinier analyses of chromatin with different linker lengths has consistently shown that the apparent fiber diameters increase with linker length (Dunn et al., 1986; Koch et al., 1987, 1988; Williams, S. P., and J. P. Langmore, manuscript submitted for publication). The estimated diameters of chromatin from *Thyone* and *Necturus* were 43.6 and 30.8 nm, respectively (Williams, S. P., and J. P. Langmore, manuscript submitted for publication), within 4% of the estimated diameters of frozen-hydrated specimens (43.5 and 32.0 nm). These data also indicated that fixation with 1% glutaraldehyde does not change the diameter. We conclude that the limited number of uniform diameter chromatin fiber segments measured by cryo-EM were representative of the bulk native chromatin.

A low-angle scattering band at ~20 nm was documented in living cells, nuclei, and chromatin solutions, and has been related to the fiber diameter (Langmore and Schutt, 1980; Langmore and Paulson, 1983; Williams et al., 1986; Koch et al., 1988). The variable position of this spacing from chromatin of different linker lengths indicates that fiber diameter increases with linker length (Williams et al., 1986; Koch et al., 1988).

Other reflections from chromatin are much less useful in

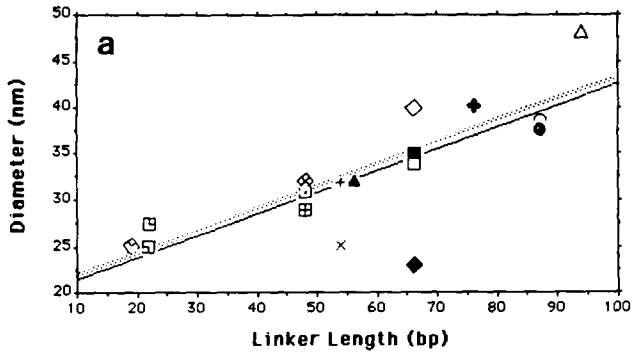

Symbol Figure 4 a	Reference #	Symbol Figure 4 a	Reference #
△	Zentgraf and Franke (1984)	+	Zentgraf and Franke (1984)
○	Williams et al. (1986)	×	Thoma et al. (1979)
●	Smith et al. (1989)	⊞	Williams et al. (1986)
✦	Giannasca and Woodcock (1988)	⊗	Giannasca and Woodcock (1988)
□	Fulmer and Bloomfield (1982)	⊡	Smith et al. (1989)
◆	Ruiz-Carrillo et al. (1980)	◳	Pearson et al. (1983)
■	Zentgraf and Franke (1984)	◱	Allan et al. (1984)
◇	Woodcock et al. (1984)	◈	Rattner et al. (1982)
▲	Zentgraf and Franke (1984)		

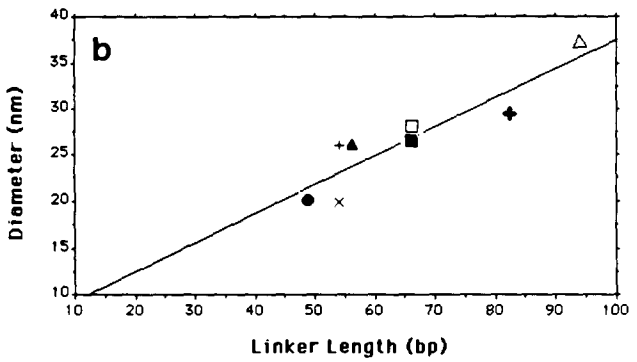

Symbol Figure 4 b	Reference #	Symbol Figure 4 b	Reference #
△	Zentgraf and Franke (1984)	▲	Zentgraf and Franke (1984)
✦	Subirana et al. (1985)	×	Derenzini (1979)
□	Zentgraf and Franke (1984)	+	Zentgraf and Franke (1984)
■	Alegre and Subirana (1989)	●	Alegre and Subirana (1989)

Figure 4. Previous EM measurements of chromatin diameter, plotted against linker length. This compilation was limited to values obtained from preparations that had salt conditions favoring formation of higher order structure. (*a*) Data from negatively stained, positively stained (and shadowed), and unstained (freeze-dried) chromatin fibers. The solid line represents the linear regression to the data: $D = 19.1 + 0.24\,n$. The dotted line represents the relationship between fiber diameter and linker length determined by Williams et al. (1986): $D = 19.3 + 0.23\,n$. (*b*) Data from embedded and stained chromatin fibers. The solid line represents the linear regression to the data: $D = 6.4 + 0.31\,n$. Refer to the tables below each plot to relate the symbols to the source of individual data points.

understanding the outer dimensions of chromatin fibers. Very low-angle "30–40 nm" reflections were seen in living cells, nuclei, metaphase chromosomes, and chromatin gels (Langmore and Schutt, 1980; Langmore and Paulson, 1983; Widom and Klug, 1985; Bordas et al., 1986*a*; Koch et al., 1987, 1988). Study of the concentration dependence led to the conclusion that the reflection was due to the side-by-side packing of the fibers, and therefore an indication of the distance between fibers rather than the fiber diameter. Therefore, even though the position of the reflection seems to be correlated with linker length (e.g., 25 nm in yeast, 33 nm in mouse lymphocytes, and 40 nm in chicken erythrocytes [Langmore and Paulson, 1983; Koch et al., 1988]) no conclusions about diameter can be drawn.

Chromatin also gives rise to diffraction bands at 11-, 6-, 3.8-, 2.7-, and 2.1-nm spacings, independent of linker length, suggesting a conserved packing of nucleosomes and DNA in the thick fiber (e.g., Olins and Olins, 1972; Langmore and Paulson, 1983; Widom and Klug, 1985; Williams et al., 1986). However, major variations in the relative contrast among those reflections (Langmore and Paulson, 1983; Williams et al., 1986) indicate that the internal structure of the fibers of different linker length are not identical.

EM of Negatively Stained, Shadowed, and Unstained Soluble Chromatin Fibers. Fig. 4 *a* is a summary of the diameters of stained, shadowed, and unstained soluble chromatin fibers presented in the literature since 1975. These measurements are plotted with linker length, *n* (bp), and fit to the equation for diameter: $D = 19.1 + 0.24\,n$ (solid line, Fig. 4 *a*). Statistical analysis indicates strong linear correlation (slope = 0.24 nm/bp; SEM = 0.05; $r_c = 0.78$; $P_c(r_c,n) < 1 \times 10^{-3}$). This fit agrees remarkably well with the relationship determined by x-ray scattering (Williams et al., 1986): $D = 19.3 + 0.23\,n$ (*dotted line*, Fig. 4 *a*). Also included in Fig. 4 *a* are diameter measurements of "superbeads" made by Zentgraf and Franke (1984). These oligonucleosome fragments are interpreted to be short segments of chromatin fibers with diameters that depend upon DNA linker length.

Negatively stained or metal-shadowed unfixed sea urchin ($n = 94$ bp), chicken erythrocyte ($n = 66$ bp), and yeast ($n = 20$ bp) fibers were studied by Widom et al. (1985) and Lowary and Widom (1989). They concluded that the diameters of those fibers were indistinguishable. Unfortunately, the method of fiber measurement was not mentioned, nor were the data shown or subjected to statistical analysis. Consequently, it is not known whether the uncertainties in their measurements might have obscured differences among their samples. The conclusion of Widom and colleagues is not supported by this cryo-EM study or the x-ray studies (discussed above). The small diameter of sea urchin fibers reported by Widom et al. (1985) might be the result of fiber unraveling, perhaps due to histone H1 loss or proteolysis, which can reduce fiber diameter (Williams, S. P., and J. P. Langmore, manuscript submitted for publication). The large diameter reported by Lowary and Widom (1989) for yeast does not agree with any of the other studies of that organism, namely an x-ray study that found a diameter of ~25 nm (Koch et al., 1987) and EM studies that found a diameter of 20-30 nm (Rattner et al., 1982; Allan et al., 1984). A major difference between the Widom studies and those reported in Fig. 4 *a* was the use of nonphysiological polyvalent ions and extremely low ionic strength. In addition, the yeast results were determined from specimens having an average DNA size of only 3.5–4 kbp (about eight times shorter than the fibers used in this, and most other, studies). For these reasons the Widom measurements were not included in the linear regression analysis.

EM of Embedded and Sectioned Chromatin. Fig. 4 *b* shows the diameter measurements of fixed, embedded, and positively stained chromatin fibers, presented in the literature since 1975, plotted against linker length (*n*). Statistical analysis indicated a strong linear correlation (slope = 0.31 nm/bp; SE = 0.06; $r_c = 0.91$; $P_c(r_c,n) < 1 \times 10^{-3}$). A comparison of the data in Fig. 4 *b* to the results of Williams et al. (1986) (*dotted line*, Fig. 4 *a*), and to those of this paper, indicates that the embedded and stained chromatin had undergone a 10–37% shrinkage. A 22% chromatin shrinkage during embedment has been estimated by x-ray scattering from chicken erythrocyte nuclei (Langmore and Paulson, 1983). Similar results (variable shrinkage up to 31%) were observed by Earnshaw et al. (1978) for embedded and stained virus particles. Despite the apparent fiber shrinkage, the sectioned chromatin clearly showed the dependence of diameter upon linker length (as noted earlier by Alegre and Subirana, 1989).

Hydrodynamic Studies Do Not Give Consistent Conclusions about Chromatin Structure

Hydrodynamic studies have the potential of answering many questions about chromatin structure. However, interpretations are subject to uncertainties regarding the flexibility, curvature, and hydration of the fibers. In addition, as in the case of x-ray studies, the measurements are always mass averages over all molecules, including some that might be aggregated, sheared, or otherwise distorted.

Thomas et al. (1986) have found that the sedimentation velocity of sea urchin sperm ($n = 94$ bp) chromatin is ~30% greater than that of rat liver ($n = 49$ bp) chromatin, under conditions that aggregation could be ruled out. That result was attributed to different flexibilities for chromatin fibers of constant diameter. Unfortunately, that hypothesis is not easily tested. Alternatively, the result can be attributed to a greater mass per unit length for the long linker chromatin, in agreement with the experimental results of Williams et al. (1986), Koch et al. (1987, 1988), and Williams, S. P., and J. P. Langmore (manuscript submitted for publication).

McGhee et al. (1983) measured the electric dichroism of chromatin with different linker lengths and concluded that the fiber diameter and mass per unit length were conserved. It is difficult to evaluate that result, because of the large discrepancies among the more than 50 optical studies made of oriented chromatin (discussed by Koch et al., 1988). Dimitrov et al. (1988) have specifically questioned the validity of the McGhee results, owing to their finding that the high electric fields used by McGhee et al. (1983) caused distortion of the chromatin.

Evidence against Fiber Aggregation

Widom and Klug (1985) observed that many chicken erythrocyte fibers prepared with polyvalent ions had diameters ≥50 nm. Upon visual inspection of these micrographs, they concluded "that any filament diameter of more than 300 Å arises from side-to-side aggregation of 300 Å filaments." This "ag-

gregation hypothesis" has been used to explain results that indicate fiber diameters >30 nm (Widom, 1989). Indeed, the micrographs of Widom et al. (1985) and Lowary and Widom (1989) do show appreciable aggregation.

The chromatin fiber segments analyzed in this study were free from apparent lateral packing, interdigitation, and bifurcation. There was no evidence of a bimodal distribution of fiber diameters in this or earlier studies performed at physiological ionic conditions (Woodcock et al., 1984; Williams et al., 1986; Smith et al., 1990). Under solution conditions identical to those used in this paper, x-ray studies show that the radii of gyration of *Thyone* and *Necturus* fibers are concentration independent, evidence that intermolecular aggregation has not occurred (Williams, S. P., and J. P. Langmore, manuscript submitted for publication).

Models for the Chromatin Fiber

The Constant-Diameter Solenoid Models. The solenoid model was originally conceived as the simplest way to form a chromosome fiber from a chain of nucleosomes (Finch and Klug, 1976). This model was supported by the observation of a 10-nm "nucleofilament" at low ionic strength, which was thought to form a helix in physiological salt. The solenoid is a single-start "contact helix" with an 11-nm pitch and a mass per unit length of five to six nucleosomes per 10 nm (Finch and Klug, 1976; Thoma et al., 1979). The solenoid model has been considered to have a constant diameter of about 30 nm, independent of DNA linker length (e.g., McGhee et al., 1983; Widom et al., 1985; Widom, 1989). The linker DNA in the solenoid model was originally proposed to be closely associated with the nucleosome core particle (Finch and Klug, 1976), or perhaps supercoiled between adjacent nucleosomes (McGhee et al., 1983), creating a hollow center (compare Fig. 5, *a* and *b*). An alternate proposal bent the linker DNA into the center of the fiber, creating a fiber with a diameter of 32.5 nm and 5.7 nucleosomes per 11 nm. In this "defined structure of the 30-nm chromatin fibre," both the diameter and mass per unit length were constant, independent of linker length (Butler, 1984). The observation of a fiber diameter that increases with linker length is unequivocal evidence against any of the constant-diameter solenoid models.

The Variable Diameter Solenoid Model. There are no apparent steric constraints that prevent a variable-diameter model to be built in the solenoid pattern. We therefore propose a variable-diameter solenoid model that seems to fit almost all of the structural data. The variable-diameter model would have linker DNA looped toward the fiber center, similar to the model of Butler (1984), but would have a variable diameter and number of nucleosomes per turn. The longer the linker DNA, the larger the radius of the fiber. By allowing the number of nucleosomes per unit length to increase with linker length the side-by-side interactions of the nucleosome cores could be conserved. This model would qualitatively agree with the diameter and mass per unit length data (Williams et al., 1986; Williams, S. P., and J. P. Langmore, manuscript submitted for publication), and with data that chromatin fibers are not hollow (Smith et al., 1990). Final evaluation of the plausibility of the variable-diameter solenoid model requires that three-dimensional models be built that do not have prohibitive steric contacts. The only evidence disfavoring the variable-diameter solenoid model are

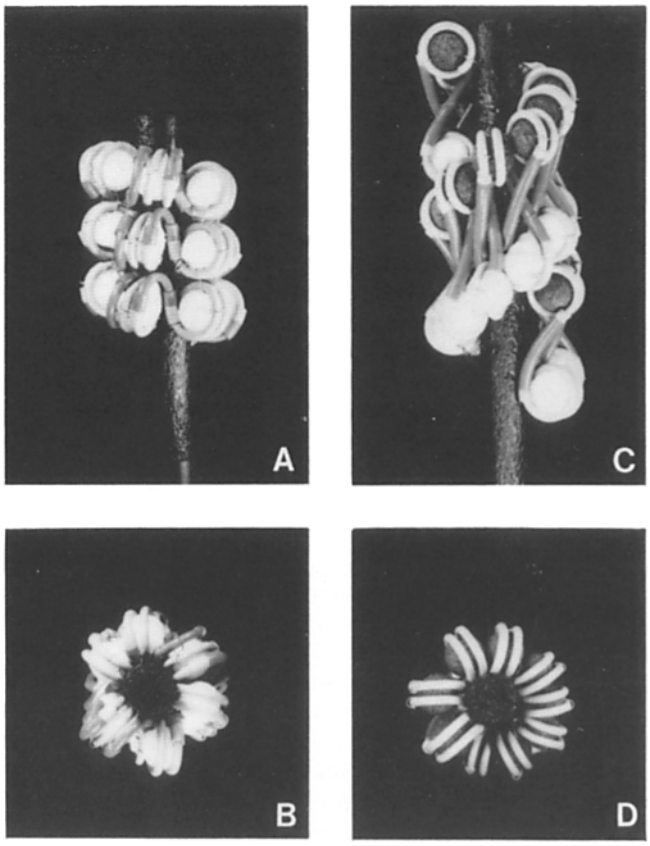

Figure 5. Space-filling models illustrating the solenoid and twisted-ribbon structures. Core DNA is shown in grey; linker DNA (n = 48 bp, as in *Necturus* erythrocytes) is shown in black. Numbers indicate the sequence of nucleosomes. (*A* and *B*) Side and end views of the hollow-solenoid model. The model has a helical repeat of six nucleosomes per 11 nm; pitch of 11 nm; diameter of 30 nm; and a central hole of 8.0 nm diameter. (*C* and *D*) Side and end views of the twisted-ribbon model, showing the single ribbon of dinucleosomes consisting of the even (*white*) and odd (*black*) nucleosome cores. The model has a helical repeat of 18 nucleosomes per 32 nm; pitch of 32 nm; diameter of 30 nm; and a central hole of 8.0 nm diameter.

(*a*) the kinetic data (Bordas et al., 1986*a*; Smirnov et al., 1988), which show that chromatin can fold very rapidly, presumably without the large change in topology required to form a solenoid; and (*b*) the Fourier transforms of negatively-stained chromatin (Williams et al., 1986), which are most consistent with double-helical symmetry.

The Twisted-Ribbon Models. The original twisted-ribbon model, proposed by Worcel et al. (1981), predicts fiber diameters of 25–30 nm, depending upon linker length, and a helical repeat that increases with linker length. A modification of this model, proposed by Woodcock et al. (1984), was arbitrarily constrained to have a constant diameter of 30 nm, but also has a helical repeat that increases with linker length. This model is shown in Fig. 5, *c* and *d*. The observation of a diameter >40 nm for *Thyone* chromatin is evidence against both of these models. Further evidence against the models comes from x-ray diffraction and EM studies. Those investigations failed to observe predicted linker length dependent changes in the apparent helical repeat of chromatin in nuclei (Langmore and Shutt, 1980; Langmore and Paulson, 1983),

Table I. Summary of Thyone and Necturus Chromatin Estimated Diameter Measurements and Comparison to the Predictions of the Double-Helical Crossed-Linker Model

Technique	Estimated diameter		Reference
	Thyone	*Necturus*	
	(nm)		
X-ray scattering	43.6 ± 1.1	30.8 ± 1.1	Williams, S. P., and J. P. Langmore (manuscript submitted for publication)
	39.3	30.3	Williams et al. (1986)
Cryo-EM unstained, hydrated	43.5 ± 4.2	32.0 ± 3.3	This paper
CTEM negative stain	37.8 ± 3.8	30.0 ± 3.1	Williams et al. (1986)
	–	31.9 ± 3.7	Giannasca, P. J., and C. L. F. Woodcock 1988. *J. Cell Biol.* 107:312a.
STEM unstained, dehydrated	38.0 ± 3.7	31.2 ± 3.6	Smith et al. (1990)
Computer models	45.0*	31.0*	This paper
Physical models	44.6*	30.0*	Smith et al. (1990)
		33.0‡	Williams et al. (1986)

* Measurement of the $\Delta L = -2$ model.
‡ Measurement of the $\Delta L = -1$ model.

concentrated gels (Widom and Klug, 1985; Widom et al., 1985), and in Fourier transforms of negatively stained fibers (Williams et al., 1986). Both twisted-ribbon models are also inconsistent with the observation of an increase in mass per unit length with linker length (Williams et al., 1986; Williams, S. P., and J. P. Langmore, manuscript submitted for publication), because the twisted-ribbon models predict a decrease in mass per unit length with increasing linker length. The Woodcock model is further discounted because it is hollow, in disagreement with scanning transmission EM (STEM) results (Smith et al., 1990). We cannot propose any modification to the twisted-ribbon models that could make them agree with the mass per unit length or helical repeat data.

The Crossed-Linker Models

THE CROSSED-LINKER MODELS PREDICT FIBER DIAMETERS THAT INCREASE WITH LINKER LENGTH

The crossed-linker models are characterized by nonsequential arrangements of nucleosome cores connected by transverse linker DNA. These models are compatible with the EM observation that unfolded chromatin has a zig-zag appearance at low ionic strength (Thoma and Koller, 1977; Worcel et al., 1981; Woodcock et al., 1984). (The earlier observations of a 10-nm nucleofilament at low ionic strength have been attributed to specimen preparation artifacts [Worcel et al., 1981; Widom, 1989].) The zig-zag structure is consistent with neutron scattering (Suau et al., 1979), x-ray scattering (Koch et al., 1987), STEM analysis (Woodcock et al., 1984), and cryo-EM (Dubochet et al., 1988) studies. The diameter increase with linker length is an obvious consequence of the zig-zag crossing the chromatin fiber axis. We used the term "crossed-linker" to describe models built in this way (Williams et al., 1986).

The crossed-linker models can be partially described by the number of helical gyres, n, in each helical repeat. Staynov (1983) was the first to describe a crossed-linker model; the proposed "nonsequential" models were single-start (n = 1) helices. Other crossed-linker models (n = 2, 3, and 5) have also been proposed (Makarov et al., 1985; Williams et al., 1986; Bordas et al., 1986*b*; reviewed by Koch, 1989). The specific path of linker DNA, the absolute fiber diameters, the radial distribution of density within the fibers, and the allowed orientations of nucleosome cores are different for each of these crossed-linker models. The recent finding of relatively straight linker DNA (compared to kinked nucleosomal DNA) in rat liver chromatin by probing the formation of photo-induced thymine dimers by Pehrson (1989) is in support of the crossed-linker class of models, which specify straight lengths of linker DNA.

Fully compacted left-handed double-helical (n = 2) *Thyone* (n = 87 bp) and *Necturus* (n = 48 bp) computer models are shown in Fig. 6, *d*, *e*, *i*, and *j*. They have a linking number increment of $\Delta L = -2$ per nucleosome. The models were built with straight linker DNA and thus have the maximum possible diameter (alternative, curved paths for the linker DNA could give rise to smaller diameters without changing the helical parameters). Measured edge-to-edge, the straight-linker models predict diameters of 45.0 and 31.0 nm for *Thyone* and *Necturus*, respectively; within 3% of the estimated diameters determined by cryo-EM and within 1% of those determined by x-ray diffraction (Williams, S. P., and J. P. Langmore, manuscript submitted for publication). A summary of *Thyone* and *Necturus* chromatin estimated outer diameter measurements and model predictions is presented in Table I.

A HYPOTHETICAL COMPACTION OF THE ZIG-ZAG RIBBON

The left-handed double-helical crossed-linker model has many features that are not easily appreciated by modeling the compacted fiber alone. Therefore, computer simulations of the folding of *Thyone* and *Necturus* chromatin are shown in Fig. 6, *a–i*. In its fully extended form, the double-helical fiber appears as a zig-zag ribbon of nucleosomes that are oriented with the flat faces parallel to the long axis of the fiber (Fig. 6, *a* and *f*). Compaction of the zig-zag into the double-helical fiber can be considered to be comprised of two independent steps. First, the ribbon (Fig. 6, *a* and *f*) is

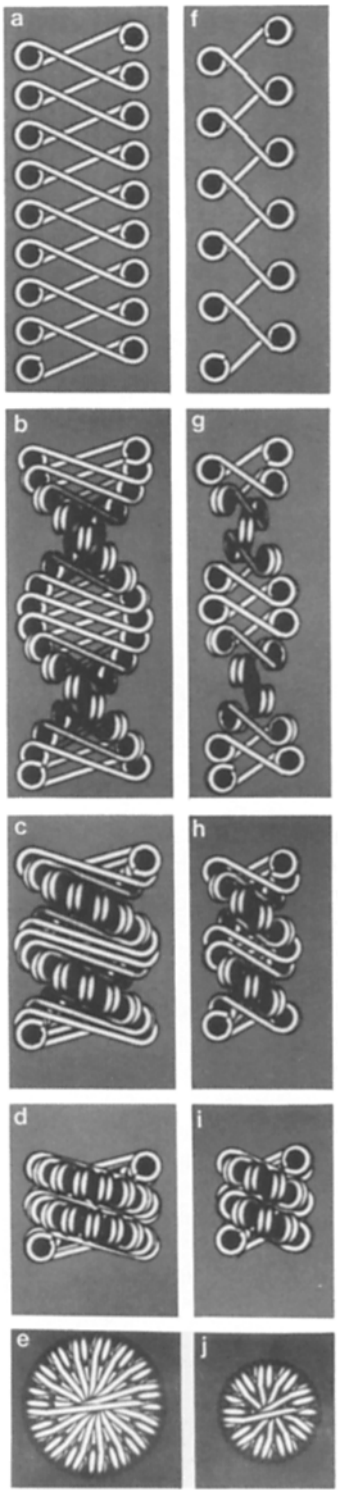

Figure 6. A computer-modeled compaction of $\Delta L = -2$ zig-zag nucleosomal ribbons of (n = 87 bp) and (n = 48 bp) into *Thyone* sperm (*a–e*) and *Necturus* erythrocyte (*f–j*) double-helical crossed-linker chromatin models. The origin of the fiber diameter dependence on DNA linker length is indicated by the cross-wise disposition of linker DNA. (*a* and *f*) Extended ribbons. (*b* and *c*, and *g* and *h*) Intermediate stages of folding (4× and 2× the double-helical pitch). (*d*, *i*, *e*, and *j*) Side and end views of fully compacted *Thyone* (*d* and *e*) and *Necturus* models (*i* and *j*). The *Thyone* model has a diameter of 45.0 nm, a helical repeat of 32 nucleosomes, and a double-helical pitch of 27 nm. The *Necturus* model has a diameter of 31.0 nm, a helical repeat of 20 nucleosomes, and a double-helical pitch of 26 nm.

twisted to form an open left-handed helix (Fig. 6, *b* and *g*). Second, it is compacted axially (Fig. 6, *c* and *h*), eventually forming the fully compacted thick fiber structure (Fig. 6, *d*, *e*, *i*, and *j*).

This hypothetical folding sequence is consistent with most EM and solution scattering experiments. Electron micrographs at low ionic strength (Thoma et al., 1979; Worcel et al., 1981; Woodcock et al., 1984) show a marked tendency of chromatin to form flat, open zig-zags. As ionic strength is increased, this zig-zag structure gradually becomes more compact (Thoma et al., 1979; Woodcock et al., 1984). At intermediate ionic strengths, the fibers appear to be composed of a series of small beads (compare Fig. 6, *c* and *h*); these structures provide a plausible explanation for the common observation of "superbead" fibers (e.g., Zentgraf et al., 1984). Also observed at intermediate stages of folding are fibers with an apparent helical gyre spacing and angle which is larger than those found in the fully compacted model (compare Fig. 6, *c*, *d*, *h*, and *i*). For example, a ~14-nm spacing was observed in chicken erythrocyte fibers (n = 66 bp) (Woodcock et al., 1984) at the intermediate ionic strength of 20 mM salt. The helical symmetry of the models is consistent with the interpretation of Fourier transforms of electron micrographs (Williams et al., 1986).

During the folding, the radius of gyration and diameter of the model increase slightly while the mass per unit length increases dramatically. This is in agreement with neutron (Suau et al., 1979; Dunn et al., 1986) and x-ray scattering (Koch et al., 1987, 1988) results, and STEM mass per unit length analysis (Woodcock et al., 1984). On the other hand, the neutron scattering study of Gerchman and Ramakrishnan (1987) concluded that the radius of gyration of chicken erythrocyte fibers increased in proportion to the mass per unit length.

The absolute mass per unit lengths of the fully compacted *Thyone* and *Necturus* models are in excellent agreement with STEM (Williams et al., 1986) and solution scattering results (Williams and Langmore, manuscript submitted for publication) obtained from isolated fibers prepared under conditions identical to those used for this diameter study. Other studies indicate consistently lower values for the mass per unit length (e.g., Suau et al., 1979; Greulich et al., 1987). However, as shown in Fig. 6, the mass per unit length of the crossed-linker models would depend strongly upon the degree of condensation, which might vary with salt conditions, stoichiometry of histone H1, and other variables. The crossed-linker models could derive their stability from interactions among linker DNA segments, allowing regular structure to form at intermediate levels of compaction, as seen by many x-ray studies at low ionic strength (e.g., Sperling and Klug, 1977; Bordas et al., 1986*a*).

The best experimental evidence consistent with this hypothetical folding sequence comes from x-ray and optical studies (Bordas et al., 1986*a*; Smirnov et al., 1988; discussed in Widom, 1989). These investigations showed that the folding and unfolding process of high molecular weight chromatin fibers is extremely rapid, occurring in <10 ms. Additionally, it has been shown that reversible folding of intact chromatin fibers can take place inside nuclei simply upon modulation of salt concentration (Olins and Olins, 1972; Bordas et al., 1986*a*), apparently independent of topoisomerase activity. As seen in Fig. 6, a very small change in the linking number increment ($\Delta L = -0.05$ per nucleosome folded in the case of *Necturus*) and no change in the orientation of the nucleosome core is required for the folding of the double-helical crossed-linker model (Williams et al., 1986). In addition, these models can be built with either the $\Delta L = -1$ or $\Delta L = -2$ zig-zag ribbons (Williams et al., 1986). In contrast, compaction of solenoid models from either zig-zag ribbon requires a large change in the topology of the DNA, which is expected to slow the folding reaction.

The Heterogeneity of Chromatin Fiber Diameter and Linker Length

Until completion of this cryo-EM study, we had mistakenly assumed that the apparent irregularity in diameters of negatively stained chromatin was due to artifacts of specimen preparation, such as dehydration, fixation, or surface denaturation (Williams et al., 1986). In general, hydrodynamic and x-ray scattering cannot measure variations in structure, but only measure mass average values. An exception was the study by Williams et al. (1986), which determined that the width of the "20-nm" reflection from *Necturus* and *Thyone* was consistent with a 22% standard deviation of the diameter. Cryo-EM was able to measure individual fiber diameters and quantitate the irregularity that is inherent to chromatin. The error analysis of the diameter data indicated that the standard deviations of the chromatin measurements were three to five times higher than those of the TMV measurements. Also, the standard deviation in the chromatin data was ~10% of the mean, whereas the standard deviation in the TMV data was only ~5% of the mean. Because the contrast in the chromatin images was much greater than that of TMV (due to the greater mass per unit length and greater amount of nucleic acid), the experimental error in the chromatin measurements should have been less than in the virus measurements. Therefore, we conclude that the observed variations in the chromatin measurements were due to inherent variations in the diameter of *Thyone* and *Necturus* chromatin fibers. The same conclusion can be drawn from the STEM studies of Smith et al. (1990).

The origins of these variations are uncertain. A reasonable hypothesis is that the variations in diameter are related to variations in linker length, in the same way that the average diameters are related to the average linker lengths. The empirical relationships between average diameter and average linker length (compare Fig. 4 *a* and Williams et al., 1986) indicate that the diameter increases by 0.23 nm for every base pair increase in the DNA linker length. Using this relationship, the observed 4.2-nm standard deviation in the diameter of *Thyone* chromatin could be attributed to a standard deviation of 18 bp in the linker length. Likewise, the observed 3.0-nm standard deviation in the diameter of *Necturus* chromatin could be attributed to a standard deviation of 13 bp in the linker length. These values are surprisingly similar to measurements of the variability in linker length. EM measurements of the center-to-center distances of nucleosome cores in calf thymus chromatin gave an apparent linker length standard deviation of 20 bp (Langmore and Wooley, 1975) and 22–28 bp (Martin et al., 1977). Gel electrophoresis of rat liver nucleosome dimers and trimers gave a standard deviation of 17 bp (Strauss and Prunell, 1982). Analysis of the chicken erythrocyte sequence data of Satchwell and Travers (1989), which included 26 trimmed dimers longer than 312 bp (i.e., the minimum length of a chromatosome dimer), gave a standard deviation of 23 bp in apparent linker length. Thus, it is reasonable that the variation in fiber diameters could be the direct result of variations in linker length within a tissue.

There are two models for linker heterogeneity. (*a*) The linker lengths could be locally uniform, but vary from region to region in the genome. (*b*) The linker lengths could be locally heterogeneous. Local uniformity could give rise to domains of structural order, but variations in structure in different regions of the genome. Local heterogeneity could give rise to local disorder. Unfortunately, the spatial distribution of linker length is not known. It is impossible to use our cryo-EM data to explore this issue, because we have biased the result by selection of fibers on the basis of local uniformity. Martin et al. (1977) addressed this issue by nuclease digestion and EM of calf thymus chromatin, and concluded that the lengths of adjacent linkers were correlated. However, Strauss and Prunell (1982) carefully analyzed the molecular weight distributions of nuclease-trimmed H1-containing dimer and trimer fragments from rat liver, and concluded that the majority of adjacent linker lengths were uncorrelated. Additionally, nucleosome mapping by indirect end-labeling has shown local heterogeneity to be the rule near structural genes (e.g., Worcel et al., 1983; Udvardy and Schedl, 1984). Thus, with the exception of special sequences such as satellite DNA, local variations in linker length (and by inference, diameter) are very likely.

Thus far, all the models that have been proposed for the chromatin fiber have been built with a constant linker length. Local heterogeneity in linker length would cause nonuniformities with different characteristics in each of the models for chromatin. The solenoid model of Butler (1984), or the variable-diameter solenoid that we propose, could be built with conserved core–core interactions, with variable amounts of DNA looping into the center. In contrast, the hollow solenoid model of McGhee et al. (1983), shown in Fig. 6, *a* and *b*, could only be built with heterogeneous lengths of linker DNA separating the cores, which would not allow regular interactions among the nucleosome cores or linkers. The twisted-ribbon models would also have heterogeneous core–core interactions, but could be stabilized by conserved linker contacts. Crossed-linker models could be built with conserved linker-linker contacts at the fiber center (perhaps mediated by histone H1), and weak contacts among the nucleosome cores at the periphery. An interesting feature of a variable-linker length crossed-linker model is that the higher order structure could not be stabilized by core–core contacts. Thus, a structure is predicted which might be independent of posttranslational modification of the core histones, or to the binding of nonhistone proteins (such as HMG-17) to the core particles. Regardless of the model chosen, local heterogeneity of linker length suggests new ways to account for the fact that chromatin fibers are not rigid, highly periodic structures.

TMVs were kindly provided by Dr. T. Shuster, University of Connecticut, Storrs, and Dr. D. L. D. Casper, Brandeis University. The Bioimage Visage-2000 was kindly provided by Dr. S. Hanash and R. Kuik, The University of Michigan Medical School. Thanks also to Dr. A. Travers for kindly providing the sequences of the nucleosome dimers. We thank Edward Omron for word processing assistance; and Diane Alessi, Paul Chuba, and members of the Langmore laboratory for useful and insightful comments.

These studies were supported by National Institutes of Health (NIH) GM27937 and National Science Foundation DIR-8706052 to J. P. Langmore. B. D. Athey was supported by NIH predoctoral training grant T32 GM07315.

Received for publication 13 November 1989 and in revised form 18 April 1990.

References

Alegre, C., and J. A. Subirana. 1989. The diameter of chromatin fibers depends

on linker length. *Chromosoma (Berl.).* 98:77–80.
Allan, J., D. C. Rau, N. Harborne, and H. Gould. 1984. Higher order structure in a short repeat chromatin. *J. Cell Biol.* 98:1320–1327.
Anderson, T. F. 1951. Techniques for the preservation of three-dimensional structure in preparing specimens for the electron microscope. *Trans. NY Acad. Sci. Ser. II.* 13:130–134.
Bevington, P. R. 1969. Data Reduction and Error Analysis for the Physical Sciences. McGraw-Hill Inc., New York. 119–122, 311.
Bordas, J., L. Perez-Grau, M. H. J. Koch, M. C. Vega, and C. Nave. 1986*a*. The superstructure of chromatin and its condensation mechanism. I. Synchrotron radiation x-ray scattering results. *Eur. Biophys. J.* 13:157–173.
Bordas, J., L. Perez-Grau, M. H. J. Koch, M. C. Vega, and C. Nave. 1986*b*. The superstructure of chromatin and its condensation mechanism. II. Theoretical analysis of the x-ray scattering patterns and model calculations. *Eur. Biophys. J.* 13:175–185.
Butler, P. J. G. 1984. A defined structure of the 30 nm chromatin fibre which accommodates different nucleosomal repeat lengths. *EMBO (Eur. Mol. Biol. Organ.) J.* 3:2599–2604.
Crane-Robinson, C., D. Z. Staynov, and J. P. Baldwin. 1984. Chromatin higher order structure and histone H1. *Comments Mol. Cell. Biophys.* 2:219–265.
Derenzini, M. 1979. Fine structure of chromatin as visualized in thin sections with the Gautier selective stain for DNA. *J. Ultrastruct. Res.* 69:239–248.
Dimitrov, S. I., I. V. Smirnov, and V. Makarov. 1988. Optical anisotropy of chromatin. Flow linear dichroism and electric dichroism studies. *J. Biomol. Struct. & Dyn.* 2:1135–1148.
Dubochet, J., M. Adrian, J. Chang, J.-C. Homo, J. Lepault, A. W. McDowall, and P. Schultz. 1988. Cyro-electron microscopy of vitrified specimens. *Q. Rev. Biophys.* 21:129–228.
Dunn, S. P., J. P. Baldwin, L. Wyns, S. Muyldermans, L. Lasters, G. A. Poland, D. Z. Staynov, H. W. E. Rattle, and M. J. Wood. 1986. Neutron scattering of chromatin multinucleosomes. *Physica.* 136B:265–267.
Earnshaw, W. C., J. King, and F. A. Eiserling. 1978. The size of the bacteriophage T4 head in solution with comments about the dimension of virus particles as visualized by electron microscopy. *J. Mol. Biol.* 122:247–253.
Erickson, H. P., and A. Klug. 1971. Measurement and compensation of defocusing and aberrations by Fourier processing of electron micrographs. *Philos. Trans. R. Soc. Ser. B.* 261:105–118.
Felsenfeld, G., and J. D. McGhee. 1986. Structure of the 30 nm chromatin fiber. *Cell.* 44:375–377.
Ferrin, T. E., C. C. Huang, L. E. Jarvis, and R. Langridge. 1988. The MIDAS display system. *J. Mol. Graphics.* 6:13–37.
Finch, J. T., and A. Klug. 1976. Solenoidal model for superstructure in chromatin. *Proc. Natl. Acad. Sci. USA.* 73:1897–1901.
Fukami, A., and A. Kôichi. 1965. A new method of preparation of a self-perforated micro plastic grid and its applications (I). *J. Electron. Microsc.* 14:112–118.
Fulmer, A. W., and V. A. Bloomfield. 1982. Higher order folding of two different classes of chromatin isolated from chicken erythrocyte nuclei: a light scattering study. *Biochemistry.* 21:985–992.
Gerchman, S. E., and V. Ramakrishnan. 1987. Chromatin higher-order structure studied by neutron scattering and scanning transmission electron microscopy. *Proc. Natl. Acad. Sci. USA.* 84:7802–7806.
Greulich, K. O., E. Wachtel, J. Ausio, D. Seger, and H. Eisenberg. 1987. Transition of chromatin from the "10 nm" lower order structure, to the "30 nm" higher order structure as followed by low angle x-ray scattering. *J. Mol. Biol.* 193:709–721.
Kellenberger, E., E. Carlemalm, and W. Villiger. 1986. Physics of the preparation and observation of specimens that involve cryoprocedures. *In* Science of Biological Specimen Preparation. O. Johari, editor. SEM Inc., Chicago. 1–20.
Koch, M. H. J. 1989. Structure and condensation of chromatin. *In* Protein-Nucleic Acid Interactions. W. Saenger and U. Heinemann, editors. MacMillan Press, London. In press.
Koch, M. H. J., M. C. Vega, Z. Sayers, and A. M. Michon. 1987. The superstructure of chromatin and its condensation properties. III. Effect of monovalent and divalent cations x-ray solution scattering and hydrodynamic studies. *Eur. Biophys. J.* 14:307–319.
Koch, M. H. J., Z. Sayers, A. M. Michon, R. Marquet, C. Houssier, and J. Willfuhr. 1988. The superstructure of chromatin and its condensation mechanism. V. Effect of linker length, condensation by multivalent cations, solubility, and electric dicroism properties. *Eur. Biophys. J.* 16:177–185.
Kornberg, R. D. 1977. Structure of chromatin. *Annu. Rev. Biochem.* 46:931–954.
Langmore, J. P., and J. C. Wooley. 1975. Chromatin architecture: investigation of a subunit of chromatin by darkfield electron microscopy. *Proc. Natl. Acad. Sci. USA.* 72:2691–2695.
Langmore, J. P., and C. Schutt. 1980. The higher order structure of chicken erythrocyte chromosomes *in vivo*. *Nature (Lond.).* 288:620–622; 291: 359–360.
Langmore, J. P., and J. R. Paulson. 1983. Low angle x-ray diffraction studies of chromatin structure in vivo and in isolated nuclei and metaphase chromosomes. *J. Cell Biol.* 96:1120–1131.
Lepault, J. 1985. Cryo-electron microscopy of helical particles TMV and T4 polyheads. *J. Microsc.* 140:73–80.
Lowary, P. T., and J. Widom. 1989. Higher-order structure of Saccharomyces cerevisiae chromatin. *Proc. Natl. Acad. Sci. USA.* 86:8266–8270.
Makarov, V., S. Dimitrov, V. Smirnov, and I. Pashev. 1985. A triple helix model for the structure of chromatin fiber. *FEBS (Fed. Eur. Biochem. Soc.) Lett.* 181:357–361.
Martin, D. Z., R. D. Todd, D. Lang, P. N. Pei, and W. T. Garrard. 1977. Heterogeneity in nucleosome spacing. *J. Biol. Chem.* 252:8269–8277.
McGhee, J. D., J. M. Nickol, G. Felsenfeld, and D. C. Rau. 1983. Higher order structure of chromatin: orientation of nucleosomes within the 30 nm chromatin solenoid is independent of species and spacer length. *Cell.* 33:831–841.
Nermut, M. V. 1972. Negative staining of viruses. *J. Microsc.* 96:351–362.
Olins, A. L., and D. E. Olins. 1974. Spheroid chromatin units (μ-bodies). *Science (Wash. DC).* 183:330–332.
Olins, D. E., and A. L. Olins. 1972. Physical studies of isolated eucaryotic nuclei. *J. Cell Biol.* 53:715–736.
Olson, N. H., and T. S. Baker. 1989. Magnification calibration and the determination of spherical virus diameters using cryo-microscopy. *Ultramicroscopy.* 30:281–298.
Paulson, J. R., and J. P. Langmore. 1983. Low angle x-ray diffraction studies of HeLa metaphase chromosomes: effects of histone phosphorylation and chromosome isolation procedure. *J. Cell Biol.* 96:1132–1137.
Pearson, E. C., P. J. G. Butler, and J. O. Thomas. 1983. Higher-order structure of nucleosome oligomers from short-repeat chromatin. *EMBO (Eur. Mol. Biol. Organ.) J.* 2:1367–1372.
Pederson, D. S., F. Thoma, and R. T. Simpson. 1986. Core particle, fiber, and transcriptionally active chromatin structure. *Annu. Rev. Cell Biol.* 2:117–147.
Pehrson, J. 1989. Thymine dimer formation as a probe of the path of DNA in and between nucleosomes in intact chromatin. *Proc. Natl. Acad. Sci. USA.* 86:9149–9153.
Rattner, J. B., C. Saunders, J. R. Davie, and B. A. Hamkalo. 1982. Ultrastructural organization of yeast chromatin. *J. Cell Biol.* 92:217–222.
Richmond, T. J., J. T. Finch, B. Rushton, D. Rhodes, and A. Klug. 1984. Structure of the nucleosome core particle at 7 Å resolution. *Nature (Lond.).* 311:532–537.
Ruiz-Carrillo, A., P. Puigdomènech, G. Eder, and R. Lurz. 1980. Stability and reversibility of higher ordered structure of interphase chromatin: continuity of deoxyribonucleic acid is not required for maintenance of the folded structure. *Biochemistry.* 19:2544–2554.
Satchwell, S. C., and A. A. Travers. 1989. Asymmetry and polarity of nucleosomes in chicken erythrocyte chromatin. *EMBO (Eur. Mol. Biol. Organ.) J.* 8:229–238.
Smirnov, I. V., S. I. Dimitrov, and V. L. Makarov. 1988. NaCl-induced chromatin condensation: application of static light scattering at 90° and stopped flow techniques. *J. Biomol. Struct. & Dynam.* 5:1127–1134.
Smith, M. F., B. D. Athey, S. P. Williams, and J. P. Langmore. 1990. Radial density distribution chromatin: evidence that chromatin fibers have solid cores. *J. Cell Biol.* 110:245–254.
Sperling, L., and A. Klug. 1977. X-ray studies on "native" chromatin. *J. Mol. Biol.* 112:253–263.
Staynov, D. Z. 1983. Possible nucleosome arrangements in the higher-order structure of chromatin. *Int. J. Biol. Macromol.* 5:3–9.
Strauss, F., and A. Prunell. 1982. Nucleosome spacing in rat liver chromatin: a study with exonuclease III. *Nucleic Acids Res.* 10:2275–2293.
Stubbs, G., S. Warren, and K. Holmes. 1977. Structure of RNA and RNA binding site in tobacco mosaic virus from 4 Å map calculated from x-ray fibre diagrams. *Nature (Lond.).* 267:216–221.
Suau, P., E. M. Bradbury, and J. P. Baldwin. 1979. Higher order structures of chromatin in solution. *Eur. J. Biochem.* 97:593–602.
Subirana, J. A., S. Munoz-Guerra, J. Aymami, M. Radermacher, and J. Frank. 1985. The layered organization of nucleosomes in 30 nm chromatin fibers. *Chromosoma (Berl.).* 91:377–390.
Thoma, F., and Th. Koller. 1977. Influence of histone H1 on chromatin structure. *Cell.* 12:101–107.
Thoma, F., Th. Koller, and A. Klug. 1979. Involvement of histone H1 in the organization of the nucleosome and of the salt-dependent superstructures of chromatin. *J. Cell Biol.* 83:403–427.
Thomas, J. O., C. Rees, and P. J. G. Butler. 1986. Salt-induced folding of sea urchin chromatin. *Eur. J. Biochem.* 154:343–348.
Toyoshima, C., and P. N. T. Unwin. 1988. Contrast transfer for frozen-hydrated specimens: determination from pairs of defocused images. *Ultramicroscopy.* 25:279–292.
Udvardy, A., and P. Schedl. 1984. Chromatin organization of the 87A7 heat shock locus of *Drosophila melanogaster*. *J. Mol. Biol.* 172:385–403.
van Holde, K. E. 1989. Chromatin. Springer-Verlag New York, Inc., New York. 292–303.
Widom, J. 1986. Physicochemical studies of the folding of the 100 Å nucleosome filament into the 300 Å filament: cation dependence. *J. Mol. Biol.* 190:411–424.
Widom, J. 1989. Toward a unified model of chromatin folding. *Annu. Rev. Biophys. Chem.* 18:365–395.
Widom, J., and A. Klug. 1985. Structure of the 300 Å chromatin filament: x-ray diffraction from oriented samples. *Cell.* 43:207–213.
Widom, J., J. T. Finch, and J. O. Thomas. 1985. Higher-order structure of long

repeat chromatin. *EMBO (Eur. Mol. Biol. Organ.) J.* 4:3189–3194.
Williams, S. P., B. D. Athey, L. J. Muglia, R. S. Schappe, A. H. Gough, and J. P. Langmore. 1986. Chromatin fibers are left-handed double-helices with diameter and mass per unit length that depend on linker length. *Biophys. J.* 49:233–248.
Woodcock, C. L. F., J. P. Safer, and J. E. Stanchfield. 1976. Structural repeating units in chromatin. I. Evidence for their general occurrence. *Exp. Cell Res.* 97:101–110.
Woodcock, C. L. F., L.-L. Y. Frado, and J. B. Rattner. 1984. The higher order structure of chromatin: evidence for a helical ribbon arrangement. *J. Cell Biol.* 99:42–52.
Worcel, A., S. Strogatz, and D. Riley. 1981. Structure of chromatin and the linking number of DNA. *Proc. Natl. Acad. Sci. USA.* 78:1461–1465.
Worcel, A., G. Gargiulo, B. Jessee, A. Udvardy, C. Louis, and P. Schedl. 1983. Chromatin fine structure of the histone gene complex of *Drosophila melanogaster*. *Nucleic Acids Res.* 11:421–439.
Zentgraf, H., and W. W. Franke. 1984. Differences of supranucleosomal organization in different kinds of chromatin: cell type-specific globular subunits containing different numbers of nucleosomes. *J. Cell. Biol.* 99:272–286.